Mapping the Role of Active Site Residues for Transducing an ATP-Induced Conformational Change in the Bovine 70-kDa Heat Shock Cognate Protein[†,‡]

Eric R. Johnson and David B. McKay*

Department of Structural Biology, Stanford University School of Medicine, Stanford, California 94305-5126

Received April 8, 1999; Revised Manuscript Received June 9, 1999

ABSTRACT: ATP binding induces a conformational change in 70-kDa heat shock proteins (Hsp70s) that facilitates release of bound polypeptides. Using the bovine heat shock cognate protein (Hsc70) as a representative of the Hsp70 family, we have characterized the effect of mutations on the coupling between ATP binding and the nucleotide-induced conformational change. Steady-state solution small-angle X-ray scattering and kinetic fluorescence measurements on a 60-kDa fragment of Hsc70 show that point mutations K71M, E175S, D199S, and D206S in the nucleotide binding cleft impair the ability of ATP to induce a conformational change. A secondary mutation in the peptide binding domain, E543K, "rescues" the ATP-induced transition for three of these mutations (E175S/E543K, D199S/E543K, and D206S/E543K) but not for K71M/E543K. Analysis of kinetics of the ATPase cycle confirm that these effects do not result from unexpectedly rapid ATP hydrolysis or slow ATP binding. Crystallographic structures of E175S, D199S, and D206S mutant ATPase fragment proteins show that the mutations do not perturb the tertiary structure of the protein but do significantly alter the protein−ligand interactions, due in part to an apparent charge compensation effect whereby mutating a (probably) negatively charged carboxyl group to a neutral serine displaces a K^+ ion from the nucleotide binding cleft in two out of three cases (E175S and D199S but not D206S).

The bovine 70-kDa heat shock cognate protein (Hsc70)[1] is a representative of the 70 kDa heat shock protein family (Hsp70s), proteins which bind and release unstructured, hydrophobic segments of polypeptide, thereby presumably suppressing polypeptide aggregation and misfolding (*1*). MgADP stabilizes complexes between peptides and Hsp70s, while binding of MgATP to Hsp70 proteins induces a conformational change (as monitored by fluorescence (*2*−*6*), proteolysis (*3*, *7*−*9*), circular dichroism (*10*), and solution small-angle X-ray scattering (SAXS) (*11*, *12*)) that facilitates peptide release. The ATPase and peptide binding activities of Hsp70s lie in two functionally and physically separable domains; structures of both an amino-terminal ATPase domain (residues 1−386 of bovine Hsc70) (*13*) and a carboxy-terminal peptide binding domain (residues 389−607 of *Escherichia coli* DnaK) (*14*) have been determined. Results of SAXS experiments on Hsc70 and its subfragments support a model whereby binding of MgATP induces a substantial contraction of the molecule in which the center-to-center separation of the ATPase and peptide binding domains decreases by approximately 14 Å (*11*). In the ATP-induced conformation, the dissociation rate for peptides increases severalfold over its value in the presence of ADP, and ATP hydrolysis is inhibited, presumably as a consequence of specific interactions between the ATPase and peptide binding domains (*15*).

The conformational change that induces peptide release occurs as a second, kinetically separable step after initial ATP binding (*4*, *6*). Estimates of the equilibrium constant for this step range from $\sim 10^{-1}$ for bovine Hsc70 to $\sim 10^{-3}$ for *E. coli* DnaK, corresponding to a net free energy difference of order ∼1−4 kcal/mol. If ATP is replaced with nonydrolyzable analogues, such as AMPPNP or γ-S-ATP, or if K^+ (which binds at two sites in the ATPase domain) is replaced with Na^+, nucleotide binding fails to induce this conformational change in Hsp70 proteins; the coupling of ATP binding to the conformational change is sensitive to minor perturbations in the nucleotide binding environment (*11*, *16*, *17*).

Although this process has been described at a phenomenological level, the molecular "coupling" mechanism by which binding of MgATP to the ATPase domain transduces a signal to the peptide binding domain that results in a large interdomain structural change is largely unknown. Hendershot and co-workers constructed an "ATP-induced conformation" mutant of hamster BiP, T37G, in which ATP binds

[†] This work was supported by Grant GM-39928 from the National Institutes of Health to D.B.M and Proposal 2240 at the Stanford Synchrotron Radiation Laboratory (SSRL), which is funded by the Department of Energy, Office of Basic Energy Sciences. The Biotechnology Program is supported by the National Institutes of Health, National Center for Research Resources, Biomedical Technology Program, and the Department of Energy, Office of Biological and Environmental Research. The costs of publication of this article were defrayed in part by the payment of page charges. This article must therefore be marked "*advertisement*" in accordance with 18 U.S.C. Section 1734 solely to indicate this fact.

[‡] Coordinates have been deposited in the RCSB Protein Data Bank, accession numbers 1QQO, 1QQM, and 1QQN for E175S, D199S, and D206S mutants, respectively.

* To whom correspondence should be addressed. E-mail: Dave.McKay@Stanford.edu. Tel.: 650-723-6589. Fax: 650-723-8464.

[1] Abbreviations: Hsc70, 70 kDa heat shock cognate protein; Hsp70, 70 kDa heat shock protein; HEPES, *N*-(2-hydroxyethyl)piperazine-*N*′-2-ethanesulfonic acid; MOPS, 3-(*N*-morpholino)propanesulfonic acid; CHES, 2-(*N*-cyclohexylamino)ethanesulfonic acid; SAXS, solution small-angle X-ray scattering.

10.1021/bi990816g CCC: $18.00
Published on Web 07/28/1999

tightly but does not induce a conformational change (*9*, *18*). Subsequent studies on mutants T13V, T13S, and T13G of the equivalent threonine residue in bovine Hsc70 demonstrated that the hydroxyl group of this residue is required for coupling ATP binding to an interdomain conformational change, thereby identifying one functional group that is required for coupling (*19*).

In this context, we have examined the participation of other residues within the nucleotide binding cleft of Hsc70 (Lys71, Glu175, Asp199, and Asp206) on the coupling mechanism by making point mutations (K71M, E175S, D199S, and D206S, whose effects on the structure and activity of the ATPase domain have been characterized previously (*20*−*22*)) and examining their properties. We demonstrate that each of these mutations eliminates the ATP-induced conformational change, as monitored by SAXS. We have utilized a 60-kDa truncation of Hsc70 that lacks the carboxy-terminal ∼100 amino acid residues for this purpose, since it mimics full-length Hsc70 in having a measurable decrease in radius of gyration when ATP binds (indicative of a conformational change), but it does not self-oligomerize like Hsc70 in solution, thereby circumventing the problem of polydispersity in experimental samples (*11*).

In addition to single point mutants, we have characterized double mutants that have a secondary E543K mutation in the peptide binding domain. This mutation eliminates a salt bridge between Glu543 and Arg469 that "latches" a helix over the peptide binding groove of the domain (*14*), with the consequence that peptide binding is weakened (i.e. peptides have a higher "off" rate than in wild-type protein) when Hsc70 is in its high peptide affinity state (*15*). At the same time, the E543K mutation shifts the equilibrium ∼2−3-fold toward the ATP-induced conformation of Hsc70, relative to wild-type protein, as demonstrated by previous work comparing the T13S and T13S/E543K mutant 60-kDa proteins, where the ATP-induced conformation was ∼0.5 kcal/mol more stable for the double mutant than for the single mutant (*19*). In this work, we show that the E543K mutation in the peptide binding domain "rescues" some, but not all, of the single point mutantions in the ATPase domain, thereby differentiating the mutations in the ATPase domain into those which have a greater influence in transducing ATP binding into a conformational change and those that have a lesser influence.

EXPERIMENTAL PROCEDURES

Expression Vectors for Mutant 60-kDa Fragment Proteins. Recombinant expression vectors derived from pT7-7 and pRSET have been described previously for ATPase fragment proteins (amino acids 1−386) with mutations K71M (*22*), E175S, D199S, and D206S (*21*), as well as for 60-kDa fragments (amino acids 1−554) of both wild type (*15*) and E543K mutant (*11*) proteins. These vectors were used as the starting point for consructing expression vectors for the single and double mutant 60-kDa fragment proteins used in this work, using standard methods. Briefly, vectors for double mutant 60-kDa proteins were constructed by excising DNA segments from the vectors encoding the 44-kDa mutant fragments and ligating the segments into plasmids coding for the 60-kDa E543K fragment, using restriction sites *Nde*I for the E175S mutation, *Cla*I and *Nco*I for the K71M mutation, and *Hpa*I and *Pvu*I for the D199S and D206S mutations. When it was recognized that lysine at position 543 was a mutation relative to the glutamic acid residue found at this position in the major fraction of natural bovine Hsc70 protein (*15*), expression vectors coding for glutamic acid at this position were constructed by excision and replacement of the coding sequence in this region with a synthetic oligonucleotide duplex, using EcoRI and HindIII sites as described. The presence of the expected mutations was confirmed by DNA sequencing.

Protein Expression and Purification. Expression of the recombinant 60-kDa proteins was induced in *E. coli* BL21-(DE3) cells by addition of 0.4 mM IPTG to exponential phase cultures. The purification protocol was similar to that described previously (*11*). Cell pellets were resuspended and sonicated in 25 mM HEPES buffer, pH 7.0. After centrifugation, the crude extracts were applied to a Q-Sepharose anion exchange column (Pharmacia) equilibrated in 25 mM HEPES, pH 7.0, and eluted with a gradient of 0−1.0 M KCl. Fractions containing the 60-kDa fragment were pooled, and bound nucleotide was removed by dialysis against 25 mM Bis-Tris, 10 mM EDTA, pH 7.0, followed by batch absorption with 1 mg/mL activated charcoal (Mallinckrodt) for 2−6 h. Charcoal was removed by centrifugation, and protein was applied to ATP−agarose (Sigma) and eluted with MgATP as described. Protein was further purified by chromatofocusing on Mono P (Pharmacia), using a gradient from 25 mM Bis-Tris, pH 7.0, to Polybuffer 74 (Pharmacia) adjusted to pH 4.0 with HCl. Gel filtration was then carried out on Superdex-75 (Pharmacia) equilibrated in 10 mM MOPS, 150 mM KCl, and 3 mM $MgCl_2$ at pH 7.0. The proteins were concentrated and stored in the same buffer at −70 °C.

ATPase Assays. All measurements of enzyme kinetics were performed at 25 °C. Readioactivity from ^{32}P-labeled ATP and ADP was quantified with a Phosphorimager:SF using the manufacturer's ImageQuant software (Molecular Dynamics).

The rate constant for steady-state ATPase activity (k_{cat}) was measured as described previously (*21*, *23*). The rate of ATP hydrolysis (k_2) was determined under single-turnover reaction conditions in 40 mM HEPES, 75 mM KCl, and 4.5 mM MgOAc as the buffer. The concentration of [α-^{32}P]-ATP (Amersham) was ≤10 nM in each experiment, and ATP hydrolysis activity was measured as a function of the concentration of 60-kDa fragment protein, with protein present in at least 100× molar excess over ATP. The hydrolysis rate was determined as the turnover rate at saturating protein concentration (*24*).

The rates of release of inorganic phosphate (P_i) derived from [γ-^{32}P]-ATP hydrolysis (k_3) were measured with nitrocellulose filter binding experiments (Amersham), and data were analyzed as described previously (*24*). Protein concentration was ≥2 μM and ATP concentration was ≤10 nM in all cases.

The rates of ADP release (k_4) were also determined with filter binding measurements. [α-^{32}P]-ATP (≤10 nM) was incubated with a >100-fold molar excess of protein for sufficient time to allow at least five ATPase turnovers, thereby allowing >99% hydrolysis of the radioactive ATP. ADP was added to a concentration of 0.5 mM and the decrease in filter-retained (protein-bound) [α-^{32}P]-ADP was monitored over

time; a single exponential was fit to the rate of loss of [α-^{32}P]-ADP, giving the ADP "off" rate constant k_4.

Fluorescence Measurements. All fluorescence measurements were performed at in 40 mM HEPES, 75 mM KCl, and 4.5 mM $Mg(OAc)_2$ adjusted to pH 7.0 with KOH. Time-resolved experiments with manual mixing were performed on an SLM 8000C spectrofluorometer (SLM-Aminco, Urbana, IL). The excitation wavelength was 290 nm (8 nm band-pass), and emission was observed at 305 nm (4 nm band-pass). The sample temperature was 25 °C. Data collection was initiated within 12 s after manual mixing in all cases. Data were analyzed by nonlinear least-squares methods found in KaleidaGraph (Synergy Software).

Stopped-flow techniques were used to monitor the change in tryptophan fluorescence after addition of ATP (*4*). A Bio DX-17MV stopped-flow ASVD spectrofluorometer (Applied Photophysics Ltd., Leatherhead, U.K.) equipped with a 150 W xenon arc lamp was used for all measurements. The slits were typically set at 1.5 mm, and the excitation wavelength was 290 nm. A SWG305 filter (CVI Laser, Albuquerque, NM) was used to observe fluorescence emission above 305 nm. All samples and the sample cell were equilibrated to 18 °C before mixing. Equal volumes of protein and ATP solutions were mixed; the final protein concentration was 3 μM in all cases, while the ATP concentration varied. Values of the ATP binding rate constant (k_1) were derived from the slopes of linear fits to apparent binding rate versus [ATP]. Each condition was repeated at least three times, and the resulting traces were averaged to improve the precision of the rate constants derived from the data.

Small-Angle X-ray Scattering. Solution X-ray scattering data were collected at beamline 4-2 at the Stanford Synchrotron Radiation Laboratory (SSRL). The photon energy was 8980 eV for all experiments. Samples were maintained at a constant temperature with a circulating bath adjusted to 20 °C. Experiments were conducted in 10 mM MOPS, 150 mM KCl, and 3 mM $MgCl_2$, and 2-mercaptoethanol was added to a final concentration of 5 mM before exposure to the X-ray beam to minimize radiation-induced aggregation of the samples. Data collection and associated corrections and analyses were done as described (*11*). Small-angle scattering was measured over a range 5×10^{-6} Å$^{-2} < s^2 < 5 \times 10^{-4}$ Å^{-2} (where $s = 2\pi \sin(\theta)/\lambda$, 2θ is the scattering angle, and λ is the X-ray wavelength). Data were typically collected in 4 cycles of 5 min exposures. Background scattering curves were measured on solutions containing buffer only and subtracted from the curves obtained with protein present after both datasets had been corrected for nonuniform detector response. The scattering patterns measured on two sides of a linear detector were averaged together for calculation of radii of gyration (R_g) values. R_g values were calculated in the Guinier approximation (*25*) using data in the range $1.0 \times 10^{-5} < s^2 < 4.2 \times 10^{-5}$.

Crystal Structure Determination of Mutant ATPase Fragments. Recombinant Hsc70 ATPase domain proteins (amino acids 1−386 of full length hsc70) of the D199S, E175S, and D206S mutants were crystallized at 4 °C with 20% poly(ethylene glycol) 8000, 1 M KCl, and 50 mM CHES/KOH, pH 9.0, in the prescence of 1 mM ATP and 5 mM $MgCl_2$. Crystals were adapted to a cryoprotectant solution that included 20% ethylene glycol in 5% increments and flash-frozen in a N_2 stream at 100 K. Data were measured with a Rigaku R-IIC image plate system using a rotating-anode X-ray source. Crystals were rotated through at least 120° using 1 or 1.2° oscillations. Data were reduced with DENZO and SCALEPACK (*26*). CNS version 0.3c was used for model refinement (*27*). The program O was used for model building (*28*). Active site ligands (ADP, P_i, K^+, Mg^{2+}, and coordinated water molecules) were omitted from the starting model (wild-type structure, PDB code 1HPM). After a one round of rigid body refinement, followed by simulated annealing from 2500 K, ligands that were apparent in electron density maps were included in the active sites of each mutant. Anomalous difference Fouriers were used to identify active site K^+ ions ($f'' = 1.07$ at $\lambda = 1.54$ Å). For each mutant, a large positive peak in the anomalous difference Fourier (>7 σ) was observed for K^+ no. 1, but a similar peak corresponding to K^+ no. 2 was observed only with D206S. A peak in the electron density at that position was modeled as a water molecule for mutants D199S and E175S. Subsequent rounds of positional refinement, *B*-factor refinement, and manual adjustments were done until no further improvements of the *R*-factor were observed. Coordinates have been deposited in the RCSB Protein Data Bank (accession numbers 1QQO for E175S, 1QQM for D199S, and 1QQN for D206S).

Table 1: Values of R_g for 60-kDa Fragment Proteins

protein	R_g(ADP) (Å)	R_g(ATP) (Å)	ΔR_g (Å)	conformational change?
WT	32.2 ± 0.2	28.6 ± 0.3	−3.6 ± 0.4	yes
E543K	32.0 ± 0.4	28.5 ± 0.3	−3.5 ± 0.5	yes
K71M	34.0 ± 0.3[a]	34.5 ± 0.3[a]	0.5 ± 0.4	no
K71M/E543K	33.1 ± 0.3	33.6 ± 0.3	0.5 ± 0.4	no
E175S	32.4 ± 0.5	31.3 ± 0.5	−1.1 ± 0.7	no
E175S/E543K	32.5 ± 0.3	28.3 ± 0.4	−4.2 ± 0.5	yes
D199S	31.8 ± 0.5	31.5 ± 0.7	−0.3 ± 0.9	no
D199S/E543K	32.7 ± 0.4	30.3 ± 0.4	−2.4 ± 0.6	yes
D206S	31.4 ± 1.8	30.4 ± 1.8	−1.0 ± 2.5	no
D206S/E543K	32.6 ± 0.6	30.7 ± 0.3	−1.9 ± 0.7	yes

[a] Measured at a single protein concentration, 4.3 (mg/mL). $\Delta R_g = R_g(\text{ATP}) - R_g(\text{ADP})$, where R_g(ATP) and R_g(ADP) are values of R_g measured in the presence of 0.5 mM ATP and ADP, respectively.

RESULTS

Solution Small-Angle X-ray Scattering. SAXS measurements were made on proteins under steady-state conditions, i.e., in the presence of 0.5 mM nucleotide (ADP or ATP). For each protein concentration used in experiments, the apparent R_g was computed using the Guinier approximation and a linear extrapolation of R_g versus concentration was used to estimate values of R_g at infinite dilution, as described previously (*11*). Values of R_g for wild type 60-kDa protein (reported previously (*15*)) and the mutant proteins are summarized in Table 1. None of the 60-kDa proteins having a single mutation in the ATPase domain show a significant decrease in R_g in the presence of ATP, as compared to ADP; the individual point mutations impair the coupling between nucleotide binding and a conformational change. However, the secondary E543K mutation in the peptide binding domain "rescues" three out of four of the mutations, in the sense that the double mutant shows a significantly smaller R_g with ATP than with ADP.

ATPase Cycle Kinetics. Values of selected rate constants of the ATPase cycle have been measured for the mutant proteins and interpreted in the framework of the kinetic

Table 2: Kinetic Constants of ATPase Activity for 60-kDa Fragment Proteins

protein	k_1 (10^5 M^{-1} s^{-1})	k_2 (s^{-1})	k_3 (s^{-1})	k_{cat} (s^{-1})
wild-type	4.3 (±0.4)	0.0017 (±0.0003)	nd	nd
E543K	8.0 (±0.8)	0.0021 (±0.0004)	0.0062 (±0.0022)	0.0016 (±0.0002)
K71M	nd	$<2 \times 10^{-6}$ [a]	nd	nd
K71M/E543K	32. (±2.7)	$<2 \times 10^{-6}$ [a]	nd	nd
E175S	nd	$\sim 1 \times 10^{-5}$ [b]	nd	nd
E175S/E543K	8.2 (±0.4)	$\sim 2 \times 10^{-5}$ [b]	nd	nd
D199S	nd	0.00055 (±0.00006)	nd	nd
D199S/E543K	7.0 (±0.8)	0.00070 (±0.00005)	0.0018 (±0.0008)	0.00037 (±0.00007)
D206S	nd	0.00048 (±0.00006)	nd	nd
D206S/E543K	6.6 (±0.1)	0.00047 (±0.00003)	0.0013 (±0.0006)	0.00020 (±0.00002)

[a] No significant ATP hydrolysis observed over background. [b] Estimated from initial 10% of reaction curve, since the reaction does not proceed to completion within 1 day. nd = not determined. Values of k_1 were determined at 18 °C; values of k_2, k_3, and k_{cat} were determined at 25 °C.

scheme discussed previously (*4*, *24*):

Scheme 1

$$E + ATP \underset{k_{-1}}{\overset{k_1}{\rightleftharpoons}} E{-}ATP \xrightarrow{k_2} E{-}ADP{-}P_i \underset{k_{-3}}{\overset{k_3}{\rightleftharpoons}} E{-}ADP + P_i \underset{k_{-4}}{\overset{k_4}{\rightleftharpoons}} E + ADP + P_i$$

Results are summarized in Table 2. In earlier work, the steady-state ATPase turnover (k_{cat}) was measured for mutants of the ATPase fragment alone. In this minimal domain, mutations of Lys71 (K71M, K71E, K71A) reduced the ATPase activity to undetectable levels (*22*), while mutations in other residues (E175Q, E175S, D199N, D199S, D206N, D206S) reduced k_{cat} one to 2 orders of magnitude from that of wild-type ATPase domain (*21*).

A similar trend is seen with single and double mutants of the 60-kDa fragment proteins. The K71M and K71M/E543K mutants have no detectable ATP hydrolysis activity. The hydrolysis rates of E175S and E175S/E543K are approximately 2 orders of magnitude slower than wild type or E543K. Hydrolysis rates for the other mutants are severalfold slower than their wild type or E543K counterparts.

The rate of P_i release was measured for E543K, D199S/E543K, and D206S/E543K and found to be approximately three times faster than hydrolysis. Values of steady state turnover were also measured for these mutants and found to be approximately equal to the hydrolysis rate in the case of E543K protein and approximately 2-fold slower for D199S/E543K and D206S/E543K. These rate constants were measured on these particular mutants for correlation with results from fluorescence experiments that are discussed below; rate constants were not measured for mutants which showed no measurable ATP-induced ΔR_g or measurable ATP hydrolysis activity.

It has been shown previously that the ATP-induced conformational change occurs in response to ATP binding (*11*, *16*), while the reverse transition to the ADP-bound conformation is predicated on product release after ATP hydrolysis (*11*, *24*). The kinetic results summarized here demonstrate that the absence in a difference in steady-state R_g values with ADP versus ATP in the SAXS experiments is not due to an unusually rapid ATP hydrolysis rate or an unusually slow ATP binding rate for any of the mutant proteins.

Fluorescence Measurements. Previous work on Hsc70 and its 60-kDa subfragment has shown a correlation between changes in the intensity of the tryptophan fluorescence and changes in the conformational state of the proteins (*4*). Specifically, when ATP binds to nucleotide-free protein, there is a rapid decrease in fluorescence intensity. The rate constant of the intensity change is linear with respect to ATP concentration, indicating a bimolecular process. Under conditions in which ATP binding is known to induce a conformational change that results in release of bound peptides, there is also a second, slower phase with rate $\sim 0.1-1.0$ s^{-1}. The rate constant of the step is independent of ATP concentration, indicating a unimolecular process. The specific molecular basis for the changes in tryptophan fluorescence is not known; however, the fluorescence apparently monitors a two-step binding reaction for ATP in which the conformational change responsible for releasing bound peptides occurs as a second, kinetically separable step after initial ATP binding. Finally, after an ATP-induced conformational change in the protein, the intensity relaxes to the value of ADP-bound protein as ATP is hydrolyzed and phosphate is released.

To corroborate the interpretation of the changes in R_g that we observe by SAXS, we have measured the kinetics of the change in tryptophan fluorescence after manual mixing of equimolar ATP and nucleotide-free protein (Figure 1; Table 3). The wild type and E543K proteins each show an initial intensity decrease of >9% when ATP binds, followed by a relaxation to the value observed for ADP-bound protein, with a rate approximately equal to k_{cat} of the ATPase cycle. The K71M and K71M/E543K mutants showed only a small change upon ATP binding, and no subsequent relaxation over a period of 30 min, consistent with the observations that (i) ATP binding does not induce a conformational change (as monitored by steady-state R_g values measured with SAXS) and (ii) ATP is not hydrolyzed, thereby preventing a return to the ADP-bound state of the protein. The E175S protein shows only a small change in fluorescence when ATP binds, while the double mutant E175S/E543K shows a larger change, consistent with SAXS results showing that ATP binding induces a conformational change in the double mutant but not the single mutant. No transition is observed for return to the ADP-bound form of either protein, and none would be expected on the time scale of the fluorescence experiments ($\leq$30 min), in view of the long half-life of the ATPase cycle ($\sim 10^3$ min). For D199S and D206S, a small initial change with no relaxation is observed, consistent with ATP binding failing to induce a conformational change. In contrast, for the double mutants D199S/E543K and D206S/E543K show a larger initial change followed by a relaxation that has a rate constant approximately equal to the k_{cat} of the ATPase cycle. The D199S, E175S, K71M, and K71M/E543K proteins show minimal fluorescence changes in

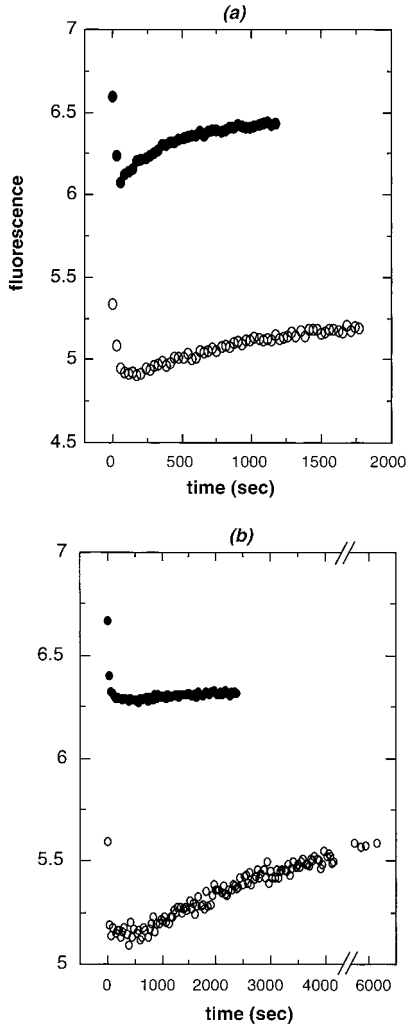

FIGURE 1: Fluorescence intensity versus time for Hsc70 60-kDa fragment proteins after addition of an equimolar amount of ATP to nucleotide-free protein. The fluorescence of 2 μM 60K fragment (1 mL) was monitored for 30 s, and the average fluorescence signal was plotted as the zero time point. Data collection was then stopped and ATP was added to yield a final concentration of 2 μM. Data collection was then restarted within 10 s, and the resulting fluorescence signal was monitored over time: (*a*) wild-type (filled circles) and E543K (open circles); (*b*) D206S (filled circles) and D206S/E543K (open circles). Plots are shifted along the vertical axis for visual comparison.

Table 3: Changes in Tryptophan Fluorescence Observed for 60-kDa Fragment Proteins

protein	% change in fluorescence: $100[F_{ATP} - F_{nucl.\ free}]/F_{nucl.\ free}$	transition rate: $F_{ATP} \rightarrow F_{ADP}$ (s^{-1})
wild-type	−14.0	0.0016 (±0.00010)
E543K	−11.0	0.0012 (±0.00003)
K71M	−3.2	no change[a]
K71M/E543K	+0.3	no change
E175S	−2.0	no change
E175S/E543K	−7.4	no change
D199S	−2.0	no change
D199S/E543K	−5.9	0.00029 (±0.00003)
D206S	−5.7	no change
D206S/E543K	−10.3	0.00021 (±0.00002)

[a] No change = no significant change observed over 30 min. All measurements done at 25 °C.

response to ATP binding, which is similar to what is observed when ADP binds to wild type protein (*4*). D206S protein showed a significantly larger (~6%) decrease in fluorescence when ATP binds; however, no significant relaxation is observed over a time course of 40 min. By comparison, D206S/E543K showed a large initial (~10%) decrease in fluroescence when ATP binds, followed by an obvious relaxation to the ADP-bound state (Figure 1). Hence, the magnitude of the fluorescence change after ATP binding, by itself, does not reveal whether the protein undergoes a conformational change. However, interpreted in conjunction with the kinetic parameters of the ATPase cycle, the kinetics of the fluorescence change following ATP binding corroborate the SAXS results in establishing which mutant proteins undergo a reversible ATP-induced conformational change.

Crystallographic Structures of Mutant ATPase Fragment Proteins. To aid in the interpretation of the mechanisms by which the mutations exert their effects, structures of the ATPase fragments of E175S, D199S, and D206S mutant proteins crystallized in the presence of KCl were solved to 1.9 Å resolution (Table 4). The structure of a K71M mutant ATPase fragment determined to 1.7 Å has been reported earlier (*22*); this structure revealed an unanticipated "charge compensation" in which mutating the (presumably) positively charged lysine side chain to a neutral methionine resulted in an additional K^+ ion binding specifically in the nucleotide binding cleft. Structures for the E175S, D199S, and D206S mutants, crystallized in the presence of NaCl, determined to 2.4 Å, have also been reported (*20*); however, due to both the lower resolution and the absence of a measurable anomalous scattering signal for Na^+ at $\lambda = 1.54$ Å, these structures did not unambiguously reveal the presence or absence of monovalent ions in the nucleotide binding cleft. Although the data collection strategy used in this work was not designed to optimize the measurement of anomalous scattering differences, a sufficient fraction of Bijvoet mates were recorded for each mutant protein to reveal peaks in anomalous difference Fouriers representing bound K^+ ions.

The overall structures of these mutants are very close to the wild-type molecule; the rms differences between wild-type and mutant C_α atoms are 0.17 Å for both E175S and D206S and 0.23 Å for D199S. Generally, some structural details of the nucleotide binding sites are less well-defined than in the wild-type structure, suggesting that the mutations introduce local disorder or multiple binding modes for neighboring ligands.

D199S. The most substantial changes in the nucleotide binding environment are observed for the D199S mutation (Figure 2b). In wild-type protein, D199 interacts with K^+ no. 2 and with two H_2O molecules in the octahedral coordination shell of the Mg^{2+} ion (Figure 2a). Mutating this residue to serine results in displacement of the K^+ ion, distortion of the Mg^{2+} octahedral coordination geometry, and displacement of the D206 side chain to an alternate conformation. The active site of the D199S mutant has density for a fully occupied Mg^{2+}ADP complex and slightly weaker but recognizable density for a P_i ion; refinement of the occupancy of P_i yields a value of 0.80, as compared to values close to 1.00 (±0.05) for ADP and Mg^{2+}. This contrasts with the structure of D199S ATPase fragment crystallized in the presence of NaCl, in which ATP is bound, presumably as a consequence of the reduced ATP hydrolysis rate in the presence of Na^+ as compared to K^+. An anomalous difference Fourier shows a large (10.3 σ) peak for K^+ no. 1 but

Table 4: Crystallographic Data Collection and Refinement Statistics for ATPase Fragment Proteins

	ATPase fragment mutation		
	D199S	D206S	E175S
unit cell params[a] (Å)			
a	143.5	143.8	143.8
b	64.2	64.4	64.0
c	46.5	46.5	46.4
resolution range (Å)	40−1.90 (2.02−1.90)[b]	40−1.90 (2.02−1.90)	40−1.90 (2.02−1.90)[b]
observns	86 567 (10 470)	91 772 (11 127)	71 438 (6596)
unique reflcns	30 759 (5255)	30 514 (4186)	29 509 (4098)
completeness	0.885 (0.921)	0.873 (0.729)	0.850 (0.719)
intensity $\langle I\rangle/\langle\sigma(I)\rangle$	23.0 (8.7)	23.8 (9.7)	17.5 (6.4)
R_{merge}[c]	0.062 (0.089)	0.038 (0.104)	0.043 (0.111)
$R_{crystallographic}$[d]	0.193 (0.258)	0.197 (0.253)	0.203 (0.267)
R_{free}[d]	0.234 (0.291)	0.230 (0.270)	0.239 (0.296)
model rms bond deviation (Å)	0.006	0.007	0.007
model rms angle deviation (deg)	1.47	1.56	1.52

[a] Space group $P2_12_12_1$. [b] Values in parentheses correspond to the highest resolution shell. [c] $R_{merge} = \Sigma|I_i - \langle I\rangle|/\Sigma\langle I\rangle$, where I = diffraction intensity and $\langle I\rangle$ = mean measured intensity. [d] $R_{crystallographic} = \Sigma|F_o - F_c|/\Sigma F_o$, where F_o = observed structure factor amplitude in working set, F_c = structure factor calculated from model, and R_{free} is the same using F_o from the test set. A test set comprised of 3% of the observed reflections was randomly selected and omitted from all model phase calculations.

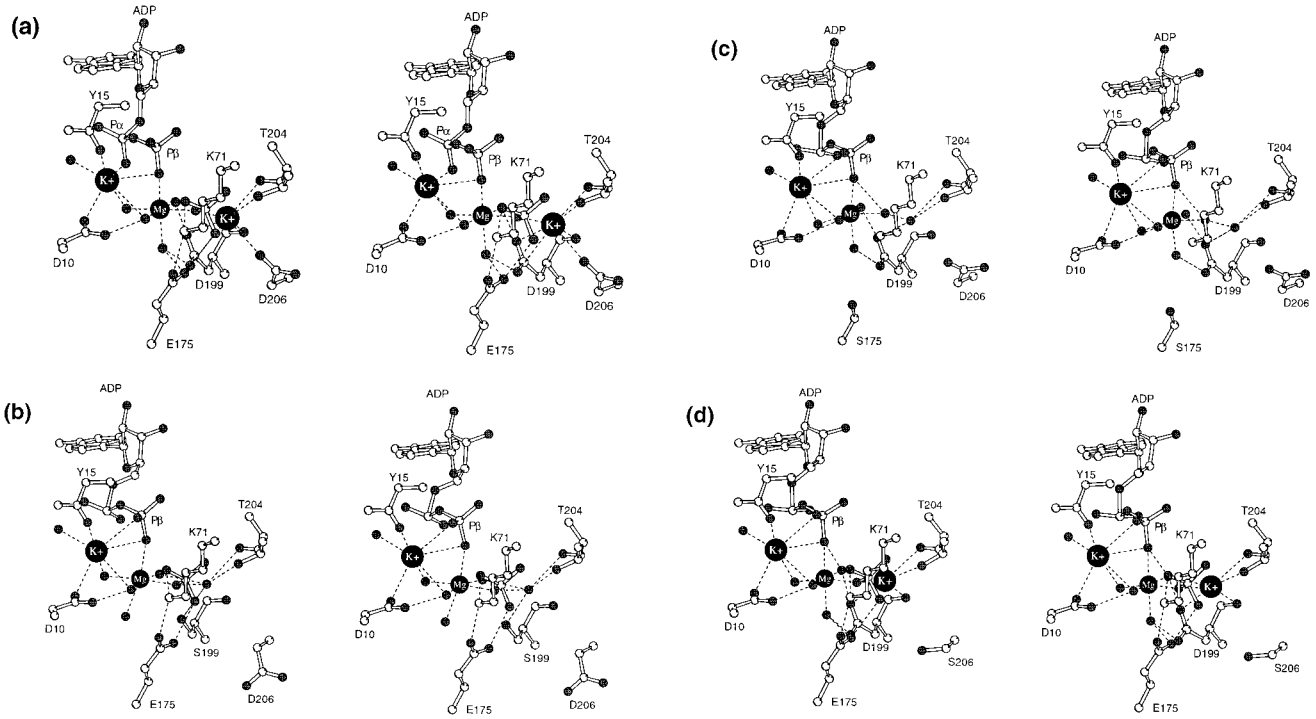

FIGURE 2: Stereoviews of the structures within the nucleotide binding region of ATPase fragment proteins, including phosphates, Mg^{2+} ion, K^+ ions, and relevant water molecules. Dashed lines show noncovalent interactions. Carbon, nitrogen, and phosphorus atoms are shown as white spheres; oxygen atoms are shown as dark spheres. The larger labeled black spheres depict Mg^{2+} and K^+ ions, and isolated dark spheres represent water molecules. Figures were drawn with MOLSCRIPT (*30*): (a) wild type (17); (b) D199S; (c) E175S; (d) D206S.

no significant signal (<3.5 σ) at the position occupied by K^+ no. 2 in the wild-type structure. Additionally, a $2F_o-F_c$ Fourier map shows a 11.4 σ peak at the position of K^+ no. 1 but only a 3.3 σ peak at the expected position for K^+ no. 2. This latter position thus appears to be occupied by a water molecule rather than a K^+ ion. The absence of the D199 carboxyl group results in a 0.9 Å displacement of one of the water molecules which coordinates the Mg^{2+} ion (at position $-z$ in Figure 2b). Additionally, the predominant conformation of the side chain of D206 is flipped "away" from the active site (although there is weak residual density suggesting minor occupancy of the normal conformation; however, only the predominant conformation could be fit and refined with confidence in the D199S model).

E175S. In the wild-type ATPase fragment, one oxygen of the E175 carboxyl group hydrogen bonds with a H_2O molecule in the $-z$ position of the Mg^{2+} inner coordination sphere and an oxygen of P_i and the other forms a salt bridge to the amino group of the K71 side chain. Mutating this residue to serine displaces the nearby K^+ no. 2; anomalous difference Fourier show a strong peak (7 σ) for K^+ no. 1 but no significant signal at the position of K^+ no. 2 (Figure 2c). $2F_o-F_c$ electron density maps indicate a mixture of Mg^{2+} ATP and Mg^{2+} ADP in the nucleotide binding site, and density in the position normally occupied by P_i is weak, suggesting that P_i only partially occupies this site or is displaced altogether. In view of this ambiguity, a solvent molecule was placed at this site. Additionally, the density

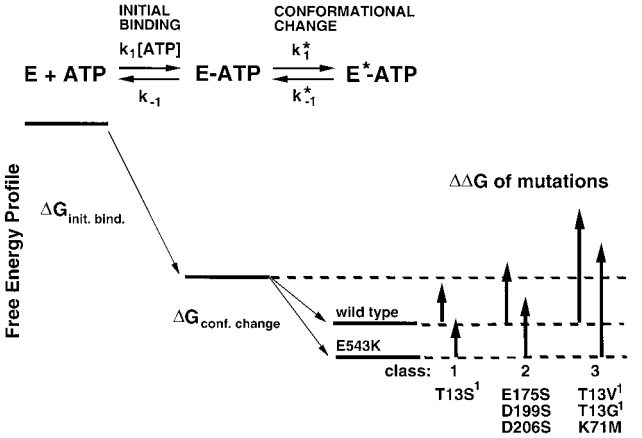

FIGURE 3: Schematic drawing of the free energy profile for ATP binding to Hsc70 and the effects of mutations. "E" represents Hsc70 60-kDa fragment protein in this case. Those marked with superscript 1 were described previously (*19*).

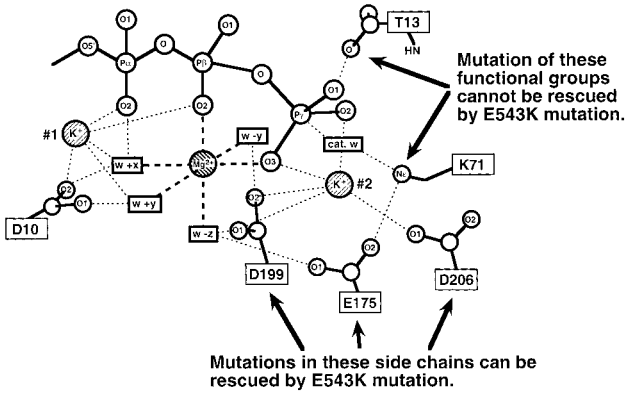

FIGURE 4: Schematic drawing of postulated molecular interactions in the nucleotide binding cleft for a precatalytic conformation of ATP. Residues whose mutation has been demonstrated to impair the ATP-induced conformational change are indicated with arrows; ability of the secondary E543K mutation in the peptide binding domain to rescue coupling between ATP binding and the conformational change is shown. Waters in the first coordination sphere of Mg^{2+} ("w") are shown as rectangles and labeled with the axis convention used previously (*20*); the putative catalytic water molecule is labeled "cat.w".

for the H_2O molecule in the $-z$ position of the Mg^{2+} cluster is weak, consistent with it being disordered.

D206S. D206 coordinates K^+ no. 2 in the wild type ATPase structure but does not interact directly with the inner sphere ligands of the Mg^{2+} ion. Mutating this residue to serine does not displace K^+ no. 2, as the other mutations did; however, it appears to result in two alternative binding sites for the ion. Anomalous difference Fouriers show a strong, ~15 σ peak for K^+ no. 1 and a ~12 σ peak at the normal position of K^+ no. 2; additionally, there is a peak of height ~6 σ displaced ~3 Å from this site, which is consistent with a minor binding site for the K^+ ion. Fully occupied Mg^{2+}ADP and P_i are present in the nucleotide binding site, and anomalous difference Fouriers show 6 σ peaks for for the phosphorus atoms of P_α, P_β, and P_i. The D206S mutation thus induces little perturbation in the nucleotide binding cleft.

DISCUSSION

Previous work provided a framework for interpreting mutations in the ATP binding domain in conjunction with the secondary E543K mutation in the peptide binding domain (Figure 3). Data have been presented that justify the scheme in which (1) ATP binding is a two-step process, (2) the second step of ATP binding induces the conformational change, and (3) the E543K mutation stabilizes the ATP-induced state in comparison to wild-type protein (*4*, *15*). This scheme predicts three classes of mutations, distinguished by their energetic effect ($\Delta\Delta G$) on ATP binding: (1) those for which the effect of the mutation in the ATPase domain on the $\Delta\Delta G$ of ATP binding is small enough that it does not impair coupling between nucleotide binding and the conformational change, either as a single mutation or in combination with the E543K mutation in the peptide binding domain (class 1, Figure 3); (2) those for which the $\Delta\Delta G$ of the mutation is large enough to inactivate the coupling between ATP binding and the conformational change for both the single and double mutation (class 3, Figure 3); (3) mutations whose $\Delta\Delta G$ values are intermediate in magnitude, for which the single mutation in the ATPase domain disables coupling but addition of the effect of the secondary E543K mutation in the peptide binding domain rescues it (class 2, Figure 3). In previous work, we presented examples of the first class of mutation (T13S and T13S/E543K) and the third class (T13V and T13V/E543K; T13G and T13G/E543K) (*19*). Here, we present examples of the intermediate class of mutations. Each of the individual mutations E175S, D199S, and D206S disables coupling between ATP binding and a conformational change, as monitored by both SAXS and fluorescence. In each case, the coupling can be rescued by introducing the secondary mutation in the peptide binding domain (E175S/E543K, D199S/E543K, D206S/E543K). It is notable that in no case have we seen the inverse effect, where a single mutation in the ATPase domain would impair coupling but addition of the E543K mutation would disable it. These data support the scheme shown in Figure 3.

In addition, we have found a second example of a residue where a mutation both disables coupling and cannot be rescued. Both the K71M single mutant and the K71M/E543K double mutant proteins are unable to undergo an ATP-induced conformational change.

The results on single and double mutations confirm the prediction that we can rank the contribution of specific residue side chains or functional groups to the coupling mechanism into three classes. It has been shown previously that a T13S mutation, which retains a hydroxyl group at position 13, affects the coupling mechanism minimally; ATP binding still induces a conformational change in both T13S and T13S/E543K mutant proteins. In contrast, removing the hydroxyl group via a T13G or T13V mutation disables coupling, and it cannot be rescued by the E543K mutation (*19*). Similarly, the K71M mutation disables coupling and cannot be rescued. This demonstrates that the interactions of the threonine hydroxyl and the lysine side chain make substantial contributions to the coupling mechanism. By comparison, the side chains of Glu175, Asp199, and Asp206 make a significant but lesser contribution, since the loss of coupling resulting from altering these residues can be rescued by the E543K mutation.

Interpretation of the specific mechanism by which each mutation exerts its effect is complicated by an apparent "charge compensation" mechanism in the nucleotide binding cleft which was first revealed in mutations of Lys71. Re-

placing the (presumably) positively charged lysine side chain with a neutral side chain resulted in a third K^+ ion binding in the cleft (*22*). In a similar vein, removing the (presumably) negative charge of an aspartic acid side chain with the D199S and E175S mutations results in loss of one of the two K^+ ions that are observed in the wild type ATPase fragment. Hence, the mutations have a global effect on the electrostatic environment, and their effects cannot be attributed solely to the alteration of specific interactions of the side chain. Adding further complexity to the interpretation, the D206S mutation does not displace a K^+ ion, so that the apparent charge compensation mechanism does not generalize to all residues. It is worth noting that these complexities contrast with the interpretation of the results of mutating Thr13, where it was possible to demonstrate that the hydroxyl group, specifically, was essential for the coupling mechanism (*19*).

In the context of this caveat, our data identify specific interactions that are crucial for transducing nucleotide binding to a conformational change. The interactions that have the greatest effect are those that have been proposed to position the γ phosphate of ATP in a "precatalytic" state (*17*), including both the interactions of the Lys71 ϵ-amino group that position a H_2O molecule for hydrolysis and a hydrogen bond of the Thr13 hydroxyl to a γ phosphate nonbridging oxygen (Figure 4). (The state we refer to as "precatalytic" here is often called a "transition state" in the literature, since the effects of nucleotide binding have been mimicked by transition state analogues in other systems. However, the long lifetime of the state ($\sim 10^2$ s) disqualifies it for a true transition state of the reaction.) Substituting Na^+ for K^+ also abolishes the ATP-induced conformational change in both wild type and E543K mutant protein; the E543K secondary mutation cannot rescue the effect of changing the monovalent ion, so that at least one, and possibly both, of the K^+ ions must participate strongly in the transduction mechanism (*11*, *15*). Notably, K^+ no. 2 would coordinate nonbridging oxygens of γ phosphate of ATP in a model that has been suggested for the precatalytic state (*17*). The carboxyl groups of Glu175, Asp199, and Asp206, which are more remote from the terminal phosphate of ATP, exert a significant but lesser effects on the transduction mechanism (Figure 4).

In vivo selection of mutants of *E. coli* dnaK has identified mutations in the nucleotide binding site that have a dominant negative phenotype. For example, in meroploid constructs, mutations E171K or D201N in one copy of the dnaK gene (which would be equivalent to E175K and D206N mutations in Hsc70) results in cells that are temperature sensitive for growth above 34 °C and which do not support growth of bacteriophage lambda (*8*, *29*). It is probable that this phenotype results from the mutant DnaK proteins being "locked" in the ADP-bound conformation (i.e. unable to transition to the ATP-induced form), with a consequent failure to release bound polypeptides efficiently in the intracellular environment. It would be of interest to determine whether the secondary mutation in the peptide binding domain, which rescues the conformational transition mechanism in vitro, would be able to suppress the effects of these mutations in the nucleotide binding site in vivo.

ACKNOWLEDGMENT

We thank Lushen Li for assistance with sample preparation, Drs. Sigurd Wilbanks, Marcelo Sousa, and Hiro Tsuruta for assistance with synchrotron data collection and interpretation, and Dr. Jeung-Hoi Ha and the Stryer Laboratory for assistance with fluorescence measurements.

REFERENCES

1. Pelham, H. R. B. (1986) *Cell. 46*, 959−961.
2. Palleros, D. R., Reid, K. L., McCarty, J. S., Walker, G. C., and Fink, A. L. (1992) *J. Biol. Chem. 267*, 5279−5285.
3. Buchberger, A., Theyssen, H., Schroder, H., McCarty, J. S., Virgallita, G., Milkereit, P., Reinstein, J., and Bukau, B. (1995) *J. Biol. Chem. 270*, 16903−16910.
4. Ha, J.-H., and McKay, D. B. (1995) *Biochemistry*. *34*, 11635−11644.
5. Banecki, B., and Zylicz, M. (1996) *J. Biol. Chem. 271*, 6137−6143.
6. Theyssen, H., Schuster, H. P., Packschies, L., Bukau, B., and Reinstein, J. (1996) *J. Mol. Biol. 263*, 657−670.
7. Liberek, K., Skowyra, D., Zylicz, M., Johnson, C., and Georgopoulos, C. (1991) *J. Biol. Chem. 266*, 14491−14496.
8. Kamath-Loeb, A. S., Lu, C. Z., Suh, W. C., Lonetto, M. A., and Gross, C. A. (1995) *J. Biol. Chem. 270*, 30051−30059.
9. Wei, J., Gaut, J. R., and Hendershot, L. M. (1995) *J. Biol. Chem. 270*, 26677−26682.
10. Banecki, B., Zylicz, M., Bertoli, E., and Tanfani, F. (1992) *J. Biol. Chem. 267*, 25051−25058.
11. Wilbanks, S. M., Chen, L., Tsuruta, H., Hodgson, K. O., and McKay, D. B. (1995) *Biochemistry 34*, 12095−12106.
12. Shi, L., Kataoka, M., and Fink, A. L. (1996) *Biochemistry*. *35*, 3297−3308.
13. Flaherty, K. M., DeLuca-Flaherty, C., and McKay, D. B. (1990) *Nature 346*, 623−628.
14. Zhu, X., Zhao, X., Burkholder, W. F., Gragerov, A., Ogata, C. M., Gottesman, M. E., and Hendrickson, W. A. (1996) *Science 272*, 1606−1614.
15. Ha, J.-H., Hellman, U., Johnson, E. R., Li, L., McKay, D. B., Sousa, M. C., Takeda, S., Wernstedt, C., and Wilbanks, S. M. (1997) *J. Biol. Chem. 272*, 27796−27803.
16. Palleros, D. R., Reid, K. L., Shi, L., Welch, W. J., and Fink, A. L. (1993) *Nature 365*, 664−666.
17. Wilbanks, S. M., and McKay, D. B. (1995) *J. Biol. Chem. 270*, 2251−2257.
18. Wei, J., and Hendershot, L. M. (1995) *J. Biol. Chem. 270*, 26670−26676.
19. Sousa, M. C., and McKay, D. B. (1998) *Biochemistry 37*, 15392−15399.
20. Flaherty, K. M., Wilbanks, S. M., DeLuca-Flaherty, C., and McKay, D. B. (1994) *J. Biol. Chem. 269*, 12899−12907.
21. Wilbanks, S. M., DeLuca-Flaherty, C., and McKay, D. B. (1994) *J. Biol. Chem. 269*, 12893−12898.
22. O'Brien, M. C., Flaherty, K. M., and McKay, D. B. (1996) *J. Biol. Chem. 271*, 15874−15878.
23. O'Brien, M. C., and McKay, D. B. (1993) *J. Biol. Chem. 268*, 24323−24329.
24. Ha, J.-H., and McKay, D. B. (1994) *Biochemistry 33*, 14625−14635.
25. Guinier, A. (1955) *Small-angle Scattering of X-rays*, John Wiley & Sons, Inc., New York.
26. Otwinowski, Z. (1990). *DENZO Data Processing Package*, Yale University, New Haven, CT.
27. Brunger, A. T., Adams, P. D., Clore, G. M., DeLano, W. L., Gros, P., Grosse-Kunstleve, R. W., Jiang, J. S., Kuszewski, J., Nilges, M., Pannu, N. S., Read, R. J., Rice, L. M., Simonson, T., and Warren, G. L. (1998) *Acta Crystallogr. D, Biol. Crystallogr. 54*, 905−921.
28. Jones, A. (1978) *J. Appl. Crystallogr. 11*, 268−272.
29. Wild, J., Kamath, L. A., Ziegelhoffer, E., Lonetto, M., Kawasaki, Y., and Gross, C. A. (1992) *Proc. Natl. Acad. Sci. U.S.A. 89*, 7139−7143.
30. Kraulis, P. (1991) *J. Appl. Crystallogr. 24*, 946−950.

BI990816G